

1 **Abstract.** The hydroxyl radical (OH) is the most important oxidant in the atmosphere and plays
2 a central role in tropospheric chemistry. Ambient OH is extremely difficult to measure because
3 of its low concentration and high reactivity. We have developed and optimized a chemical
4 ionization mass spectrometry (CIMS) system to measure OH based on ion-assisted mass
5 spectrometry. A calibration unit was developed based on chemical actinometry to convert
6 detected signals to OH concentration. Different types of ion sources (^{210}Po and corona source)
7 and scavenger gases (propane and C_3F_6) were compared. Radioactive ion source (^{210}Po foils)
8 was chosen for lower detection limits, and propane was selected for high elimination efficiency
9 and the negligible influence on the signal stability. The sensitivity of the CIMS instrument to
10 OH radicals is influenced by the efficiencies of conversion reaction, ion conversion, and ion
11 transmission. Through optimizing their efficiencies by changing the flow rates and electric
12 fields, an optimal sensitivity was determined for our system. The background noise from OH
13 interferences was reduced by adjusting the flow rate of scavenger gas. The CIMS system
14 achieved a detection limit of $\sim 0.15 \times 10^6$ molecules cm^{-3} (signal/noise=2). The CIMS was then
15 taken out to measure ambient OH at an urban site in Hong Kong in April 2019. An obvious
16 diurnal pattern of OH radicals was observed, with the highest concentration of $\sim 6 \times 10^6$
17 molecules cm^{-3} at midday and the lowest concentration of $\sim 0.25 \times 10^6$ molecules cm^{-3} at night,
18 with an overall accuracy of about $\pm 51\%$. The results demonstrated the capability of our CIMS
19 for OH measurements on clear days. The tests and results from our study provide a useful
20 reference to other researchers who wish to develop and apply the CIMS technique to measure
21 OH and other chemicals.

22

23

24

25

1 **1. Introduction**

2 The hydroxyl radical (OH) is the most important atmospheric cleansing agent, and is
3 responsible for the degradation and removal of most of trace gases (Crosley, 1997). In regions
4 strongly affected by anthropogenic activities, reactions of OH with volatile organic compounds
5 (VOCs) and carbon monoxide (CO) lead to the formation of organic peroxy (RO₂) and
6 hydroperoxyl (HO₂) radicals. They react with NO to form nitrogen dioxide (NO₂), producing
7 ozone (O₃) (e.g., Hofzumahaus et al., 2009). The reactions of OH with NO₂ and sulfur dioxide
8 (SO₂) and the self- and cross-reactions of RO₂ and HO₂ transform the primary pollutants into
9 low-vapor pressure gas molecules such as nitric acid (HNO₃), sulfuric acid (H₂SO₄), and highly
10 oxidized organic molecules (HOMs) (Lu et al., 2012). In addition, the reaction with OH is the
11 main removal pathway of methane, which is the third most important greenhouse gas according
12 to the IPCC report (Stocker et al., 2013). Therefore, OH plays key roles in major environmental
13 issues such as photochemical pollution, acid rain, haze, and climate change (Kulmala et al.,
14 2004; Wang et al., 2017; Calvert et al., 1985; Lu et al., 2019).

15 The importance of OH in tropospheric chemistry was first recognized by Levy (1971). Since
16 then, concerted efforts have been made to develop techniques to measure OH in the atmosphere
17 (Heard and Pilling, 2003). However, the low concentration, high reactivity, and short lifetime
18 (<1 s) of OH make it very difficult to be detected and quantified. The low concentration
19 requires high sensitivities and small interferences in the instruments; the high reactivity
20 demands a small loss in the sampling system, and the short lifetime requires measurement at a
21 high temporal-spatial resolution. It is a big challenge to meet all of these requirements by a
22 measurement system (Lu et al., 2019).

23 During the past decades, three major techniques have been developed for in-situ OH
24 measurements: differential optical absorption spectroscopy (DOAS) (Wennberg et al., 1990),
25 laser-induced fluorescence (LIF) (Perner et al., 1976), and chemical ionization mass
26 spectrometry (CIMS) (Eisele and Tanner, 1991). DOAS and LIF techniques directly measure
27 OH based on spectroscopic methods. The major advantage of DOAS is that it is self-calibrating
28 via the well-known Beer-Lambert law, and thus does not require to separate a calibration
29 device (Heard and Pilling, 2003). DOAS often serves as a primary standard for comparisons
30 with other measurement techniques. However, the application of DOAS to the measurement of
31 ambient OH is limited due to the interferences from other atmospheric constituents (Heard and
32 Pilling, 2003). LIF measures OH by using pulsed 308 nm single photon excitation of OH at

1 low pressure with temporally delayed detection of the OH resonant fluorescence (known as
2 fluorescence assay by gas expansion, FAGE) (Holland et al., 1995), and it requires calibration.
3 The LIF technique has the advantages of direct excitation of OH and good selectivity and
4 sensitivity (Heard and Pilling, 2003). Unlike DOAS and LIF, the CIMS technique measures
5 OH indirectly based on an ion-assisted mass spectrometry method. It employs a chemical
6 reaction scheme that OH is firstly converted into H₂SO₄ and subsequently measured by a
7 specific chem-ionization method (Eisele and Tanner, 1991). CIMS has fewer interference and
8 higher sensitivity compared to either DOAS or LIF techniques for OH measurement because
9 of the higher collection efficiency of ions than photons (Heard and Pilling, 2003). As a result,
10 CIMS processes the lowest detection limit for ambient OH measurement among the three
11 techniques (Heard and Pilling, 2003).

12 LIF has been the most widely used technique for OH measurement in laboratory and field
13 studies (Stone et al., 2012). However, some LIF instruments may suffer from interferences in
14 environments of rich VOCs and poor NO_x. Previous field measurements by LIF in forested
15 regions have observed OH concentrations that are three to five times higher than those
16 predicted by models with presently known OH sources and sinks (McKeen et al., 1997;
17 Lelieveld et al. 2008; Hofzumahaus et al., 2009; Whalley 2011; Lu et al. 2012; Mao et al. 2012;
18 Novelli et al. 2014; Feiner et al. 2016; Tan et al. 2017). The discrepancy was first attributed to
19 the existence of an unknown source of OH in VOC-rich environment (Peeters et al., 2009;
20 Hofzumahaus et al., 2009), whereas later studies found positive artifacts in some LIF
21 instruments in such environments (Mao et al. 2012; Novelli et al. 2014; Feiner et al. 2016; Liu
22 et al. 2018). For example, Mao et al. (2012) attributed 40-60% observed OH signal at a
23 California forest to an interference in their LIF by using a chemical method to remove the
24 interference. Recently, Liu et al. (2018) inferred the equivalent OH concentrations from
25 measurements of isoprene and its oxidation products over Amazon, and found that the inferred
26 OH concentrations compared well with the simulated results. On the other hand, other groups
27 did not find evidence of the positive bias in their LIF systems, which have different design and
28 configurations, continued to attribute the model underestimated OH to the presence of OH
29 unknown source(s) at their study sites (Whalley 2011; Stone et al., 2012; Fuchs et al. 2012; Lu
30 et al. 2012; Tan et al. 2017). It is highly desirable to deploy an alternative technique to re-
31 examine the OH issue in forested regions.

32 The CIMS technique for measuring OH was first developed at Georgia Institute of Technology
33 by Eisele and Tanner (1991). The system was further improved at National Center for

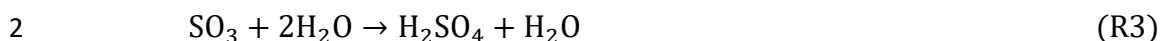
1 Atmospheric Research by reducing wall reactions (Eisele and Tanner., 1993), by reducing the
2 background signal (Tanner and Eisele., 1995), and by developing a better calibration system
3 (Tanner et al., 1997). Mauldin et al. (1998) modified the CIMS for measurement at an aircraft
4 platform during the First Aerosol Characterization Experiment (ACE1), and Edwards et al.
5 (2003) further upgraded the calibration system. Based on the design of Tanner et al. (1997),
6 another two CIMS instruments were developed at the Meteorological Observatory
7 Hohenpeissenberg, Germany, by Berresheim et al. (2000) and at the National University of
8 Ireland Galway by Berresheim et al. (2013). Kukui et al. (2008) developed a new version of
9 the CIMS instrument at the Centre National de la Recherche Scientifique (CNRS), France,
10 which allowed for OH measurements in a moderately polluted atmosphere.

11 Despite the previous development and application of CIMS for OH measurements, applications
12 of this technique remain challenging, and are hindered by a lack of detailed experimental
13 procedures to make a CIMS functional. And there have been limited deployments of CIMS for
14 ambient OH determination compared to the LIF technique, and there has been no report of OH
15 measurements by the CIMS method in Asia. In the present work, we describe here a new CIMS
16 system that has been tested and optimized at The Hong Kong Polytechnic University (PolyU).
17 The instrument was built at THS, Inc (Atlanta, Georgia) with the same design as the CIMS
18 from the group of Eisele and Tanner. The measurement principles, configurations of the CIMS
19 instrument, and a calibration unit are described in detail. Different scavenger gases, ion sources,
20 and primary ions detection was compared. In addition, the sensitivity and noise of the CIMS
21 instrument to OH radicals were tested by optimizing the flow rates and voltages. Accordingly,
22 their optimal settings were derived. Finally, the initial measurement of ambient OH
23 measurement was presented. The results presented in this work provide detailed technical
24 information for other researchers who wish to apply the CIMS to ambient OH measurement.
25 To our knowledge, this instrument is the first OH measuring CIMS in Asia.

26 **2. Measurement principles**

27 The measurement of hydroxyl radical (OH) in this study was made with a chemical ionization
28 mass spectrometry (CIMS) technique, which has been described previously (Tanner et al., 1997;
29 Sjostedt et al., 2007). Briefly, the ambient OH is converted to H₂SO₄ by adding SO₂ into the
30 sample air flow, which initiates the following reaction sequence in the presence of oxygen and
31 water vapor:



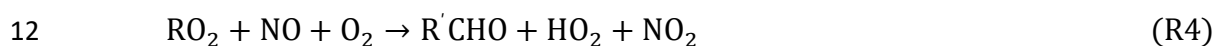


3 To mitigate interference by ambient H_2SO_4 , a scavenger gas is periodically added into the
 4 sample air flow to remove OH radicals. Then, H_2SO_4 produced from the reaction of OH and
 5 SO_2 can be obtained:

6 $[\text{H}_2\text{SO}_4]_{\text{OH}} = [\text{H}_2\text{SO}_4]_{\text{TS}} - [\text{H}_2\text{SO}_4]_{\text{BS}}$ (E1)

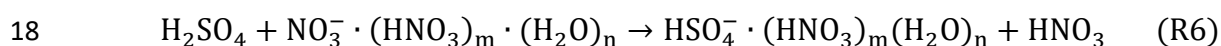
7 $[\text{H}_2\text{SO}_4]_{\text{TS}}$ and $[\text{H}_2\text{SO}_4]_{\text{BS}}$ are H_2SO_4 concentrations with and without adding scavenger gas
 8 in the front injector, respectively. (See Section 3.1.1 for details)

9 Apart from the interference from the pre-existing H_2SO_4 , the reactions of NO with ambient or
 10 Reaction 2 produced peroxy radicals ($\text{HO}_2 + \text{RO}_2$) can produce OH in the sample flow (Sjostedt
 11 et al., 2007):

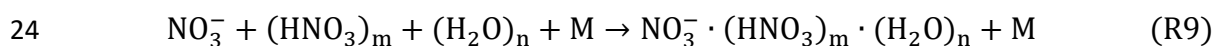


14 To reduce the positive bias from Reaction 5, another scavenger gas is added into the sample
 15 flow after SO_2 to scavenge recycled OH radicals.

16 The H_2SO_4 is then converted into HSO_4^- by chemical ionization in reaction with the NO_3^-
 17 primary reactant ions:

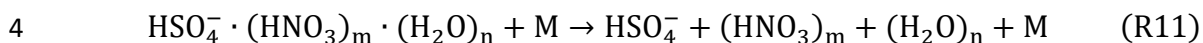
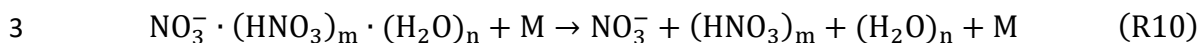


19 $\text{NO}_3^- \cdot (\text{HNO}_3)_m \cdot (\text{H}_2\text{O})_n$ are cluster ions with m and n mostly of 0-2 and 0-3 (Berresheim et
 20 al., 2000). These cluster ions are generated by the reaction of HNO_3 vapor with electrons
 21 (Fehsenfeld et al., 1975):



25 Where e^- is emitted from an ion source. The OH radical (artificial OH) formed from primary
 26 ion creation (Reaction 7) is not desirable and regards as noise signal, see details in Section

1 5.4.3. The ion clusters are subsequently dissociated by the collisional dissociation chamber
2 (CDC):



5 The OH is finally detected by a mass spectrometer system as HSO_4^- at 97 m/z.

6 **3. CIMS system**

7 Figure 1 shows the schematic of our CIMS system, which including a sample inlet system and
8 a mass spectrometer system. The sample inlet system has two regions: chemical conversion
9 region and chemical ionization region. The chemical conversion region is where H_2SO_4 formed
10 by the conversion reaction of OH and SO_2 . Then the H_2SO_4 converted in to HSO_4^- ion cluster
11 in chemical ionization region. The mass spectrometer system consists of three parts including
12 a collisional dissociation chamber (CDC) for ion cluster dissociation, an ion guide chamber
13 (IGC) to refocused the ions, and an ion detection chamber (IDC).

14 **3.1. Sample inlet**

15 As shown in Figure 1, during OH measurements, air sample at ambient temperature and
16 pressure is first drawn into a 5 cm diameter, 32 cm long stainless-steel tube. A turbulence-
17 reducing scoop is attached in the front of the tube. The flow velocity at center of the tube is 5
18 m/s, which is measured manually using a pitot. The central part of the air is then drawn through
19 a 1.6 cm diameter stainless steel inlet into the chemical conversion region with the flow rate
20 being determined by a mass flow controller (MKS, MFC company). The excess flow in the
21 tube is vented back into the atmosphere via the inlet blower.

22 **3.1.1 Chemical conversion region**

23 The chemical conversion region in Figure 1 is equipped with two pairs of stainless steel needle
24 injectors that are placed in opposite positions. The first (front injectors) pair is installed at a 69
25 mm distance from the stainless sample inlet. The distances between the first (front) and second
26 (rear) pairs are 25.8 mm. To measure OH radicals, SO_2 is continuously added into the sample
27 flow at the front injectors to convert OH into H_2SO_4 (Reactions 1-3). The purity of SO_2 is 0.9
28 vol.%.

29 As discussed above, to eliminate the ambient H_2SO_4 interference, another flow is added
30 through a zero-dead space four-way electrically operated valve, which is automatically

1 switched the injection positions of scavenger gas and pure N₂ every 3 minutes (see the pulsed
 2 flow in Figure 1). When the scavenger gas is added through the front injectors to the sample
 3 flow, N₂ is switched through the rear injectors. The CIMS is then running in background mode.
 4 Under this condition, atmospheric OH simultaneously reacts with SO₂ and the scavenger gas,
 5 with the reaction of OH with scavenger gas being much faster than SO₂. This configuration
 6 produces background signal (BS) from the interferences of atmospheric H₂SO₄ and the ion
 7 source, with negligible contribution from atmospheric OH. When the scavenger gas and N₂ are
 8 switched into the sample flow through the rear and front injectors, respectively, CIMS is
 9 running in the signal mode. Atmospheric OH is all converted by SO₂ and the total signal (TS)
 10 is produced. In addition, another flow of scavenger gas is added continuously into the sample
 11 flow through the rear injectors to scavenge OH radicals generated from Reaction 5. The OH
 12 concentration is obtained from the ratio of the difference between the total signal and the
 13 background signal to the primary ion (NO₃⁻) signal. (Tanner and Eisele, 1995):

$$14 \quad [\text{OH}] = \frac{1}{C} \times \frac{\{\text{HSO}_4^-\}_{\text{TS}} - \{\text{HSO}_4^-\}_{\text{BS}}}{\{\text{NO}_3^-\}} \quad (\text{E2})$$

15 Where the square brackets and text braces denote concentrations and signal counts, respectively.
 16 C is the calibration factor. As discussed in Berresheim et al. (2000), the absolute concentration
 17 of the H₂SO₄ and reagent ion (NO₃⁻) is not required as the OH concentration is determined
 18 based on their relative signal strength and the calibration factor.

19 **3.1.2 Chemical ionization region**

20 The sample flow through the chemical conversion region is then drawn into the chemical
 21 ionization region and mixed with the sheath gas (Figure 1). The sheath flow is continuously
 22 drawn into the same region through an annular space between 3.5 cm o.d. and 1.2 cm o.d.
 23 stainless steel tubes by a diaphragm pump (KNF-813). These tubes are concentric with the
 24 downstream end of the chemical conversion region. The sheath gas is produced by a zero-air
 25 generator (Thermo Electron Corporation, Model 111) attached with active charcoal and silica
 26 gel to remove trace gases such as SO₂ and NO_x. Before entering the ionization region, HNO₃
 27 vapor and the scavenger gas are added continuously to the sheath gas. The HNO₃ vapor is
 28 obtained by N₂ carrier gas passing through the headspace of a reservoir of concentrated liquid
 29 HNO₃. When HNO₃ doped sheath gas passes through the ion source (Figure 1), NO₃⁻ ·
 30 (HNO₃)_m · (H₂O)_n reactant ions are produced by the reaction of HNO₃ and electrons
 31 (Reactions 7-9). Additionally, the N₂ carried HNO₃ is also added through the rear injector to

1 maintain the ion cluster distribution and further improve the stability of the reagent ion signal
2 (Sjostedt et al., 2007).

3 The $\text{NO}_3^- \cdot (\text{HNO}_3)_m \cdot (\text{H}_2\text{O})_n$ reactant ions then react with H_2SO_4 molecules from the sample
4 air to form $\text{HSO}_4^- \cdot (\text{HNO}_3)_m (\text{H}_2\text{O})_n$ cluster ions in the chemical ionization region according
5 to Reaction 6. Voltages are applied to the sample and sheath flow tubes to produce an electrical
6 field to force the reactant ions to the center of the chemical ionization region and enhance the
7 interaction of reactant ions with H_2SO_4 . The optimization of voltages for better sensitivity is
8 shown in Section 5.4.2.3.

9 The total flow (Figure 1) is then exhausted at the end of the chemical ionization region through
10 diaphragm pumps (Thomas, SK-668) and controlled by an MFC. To prevent the HNO_3 vapor
11 from corroding the pump and MFC and polluting the ambient air, the exhaust flow is first
12 filtered through active charcoal cartridges and then vented back into the atmosphere at a
13 distance of >10 m from the sampling point. A small portion of the total flow is drawn into the
14 mass spectrometer system through a 101.6 μm diameter pinhole. A small counterflow of N_2
15 buffer gas is added on the atmospheric pressure side of the pinhole (Figure 1) to prevent
16 unwanted clusters and molecules from entering the pinhole (Berresheim et al., 2000). Voltages
17 are added at the positions of N_2 buffer and pinhole to force the ions into the mass spectrometer
18 system.

19 **3.2. Mass spectrometer system**

20 The mass spectrometer system is separated into three differentially pumped chambers with two
21 adjacent chambers being connected through a 4 mm pinhole (Figure 1). The first chamber
22 behind the pinhole is a collisional dissociation chamber (CDC). The pressure of the CDC is
23 typically maintained at around 0.5 hPa through a drag pump (Adixen, MDP 5011) and a scroll
24 pump (Agilent Technologies, IPD-3). The CDC has a high ion kinetic energy (i.e. high electric
25 field to number density ratio), and most of the entered cluster ions (e.g. $\text{HSO}_4^- \cdot$
26 $(\text{HNO}_3)_m (\text{HO}_2)_n$ and $\text{NO}_3^- \cdot (\text{HNO}_3)_m \cdot (\text{HO}_2)_n$) are dissociated in the CDC through
27 Reactions 10-11.

28 The second chamber is an octopole ion guide high vacuum chamber (IGC). In this chamber,
29 the pressure is maintained at about 1.3×10^{-3} hPa through a turbo molecular pump (Agilent
30 Technologies, TwisTorr 304 Fs) and the same scroll pump mentioned above. Here, the ions
31 from the CDC are refocused by an octopole ion guide and transported to the third chamber.

1 The third chamber (IDC) contains a quadrupole mass filter and detector with attached signal
2 amplifier electronics. The mass-selected ions of the quadrupole are amplified and detected by
3 a channeltron ion multiplier, and then counted based on standard techniques (Sjostedt et al.,
4 2007). This chamber maintains a pressure of about 2.6×10^{-5} hPa through another turbo
5 molecular pump and the same scroll pump.

6 **4. Calibration**

7 **4.1 Calibration principle**

8 The calibration of the CIMS (Figure 2a) is achieved by controlled concentrations of OH
9 radicals, which is produced through photolysis of water vapor by 184.9 nm light (Tanner and
10 Eisele, 1995):



13 The calibration factor C is then determined based on the produced OH concentrations and
14 detected signals of HSO_4^- and NO_3^- according to E2.

15 **4.2 Calibration unit**

16 Figure 2 shows the main components of the calibration unit. The unit is consisted by a cuboid
17 stainless steel tube, a hygrometer and an optical element. The length of the cuboid stainless
18 steel tube is 52 cm with 1.6 cm side length. The high-precision capacitance humidity
19 measurement hygrometer (Vaisala, HMP100) is connected at the front of the tube to measure
20 the temperature T and dew point temperature T_d of the mixed air. The optical elements are
21 mounted at the end of the tubes (air outlet side) to minimize the wall loss during calibration.
22 This element consists of a Pen Ray mercury lamp (Analytik Jena, UVP Pen Ray) and a
23 bandpass filter. The bandpass filter blocks most of the emitted photons except those at 184.9
24 nm. Finally, the transmitted light enters the tube and photolyzes water vapor to produce OH
25 radicals according to Reaction 12. The mixing ratio of water vapor in the air flow is controlled
26 through the mix of the dry synthetic air and humidity air from a water bubbler.

27 **4.3 Calibration quantification**

28 **4.3.1 OH quantification**

1 The concentrations of OH radicals produced from the water vapor photolysis reaction can be
2 described as follow:

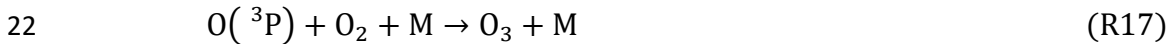
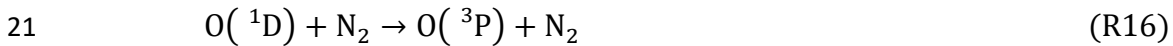
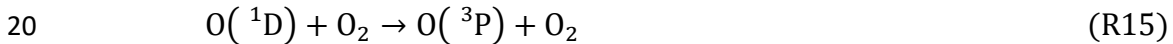
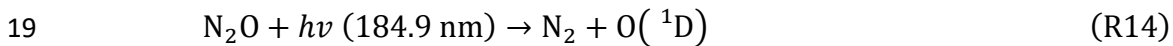
$$3 \quad [\text{OH}] = I \times t \times \sigma_{\text{H}_2\text{O}} \times \phi_{\text{H}_2\text{O}} \times [\text{H}_2\text{O}] \quad (\text{E3})$$

4 Where I and t are the photon intensity (unit: photons $\text{s}^{-1} \text{cm}^{-2}$) and the reaction time of H_2O
5 photolysis, respectively. The determination of It is described in Section 4.3.2. $[\text{OH}]$ and $[\text{H}_2\text{O}]$
6 are the concentrations of OH radicals and water vapor, respectively, $\sigma_{\text{H}_2\text{O}}$ is the photolysis
7 cross-section of water vapor at 184.9 nm ($7.22 \times 10^{-20} \text{cm}^2$, Cantrell et al., 1997) and $\phi_{\text{H}_2\text{O}}$
8 represents the photolysis quantum yield, which is assumed to be 1.0 at 184.9 nm. $[\text{H}_2\text{O}]$ is
9 calculated according to the temperature (T), saturated water vapor pressure ($P_{\text{H}_2\text{O}}^\circ$) and relative
10 humidity (RH) of the mixed air flow (Kurten et al., 2012).

11 **4.3.2 It quantification**

12 The product It is determined based on the chemical actinometry method (Figure 2b). This
13 method measures NO_x generated from N_2O photolysis with the same calibration unit under the
14 same condition as that for the CIMS calibration. Since N_2O photolysis and H_2O photolysis
15 require the same photon intensity (184.9 nm), product It of H_2O photolysis can be determined
16 by measured NO_x and N_2O mixing ratios produced by N_2O photolysis (Edwards et al., 2003).

17 Briefly, high purity N_2O (99.9%) mixed with dry synthetic gas flows into the calibration unit.
18 The photolysis of N_2O generates NO_x through the following reactions (Edwards et al., 2003):



25 The O_3 produced from Reaction 17 could oxidize NO to NO_2 . Therefore, the photolysis of N_2O
26 eventually converts it to NO_x which is concurrently measured by a commercial NO_x detector

1 (Thermo, Model 42i-TL) The combined product It is a function of the mixing ratios of N_2O ,
 2 N_2 , O_2 , and produced NO_x :

$$3 \quad It = \frac{(K_{15} \times [O_2] + K_{16} \times [N_2] + (K_{18} + K_{19}) \times [N_2O]) \times [NO_x]}{2 \times K_{18} \times \sigma_{N_2O} \times \phi_{N_2O} \times [N_2O]^2} \quad (E4)$$

4 Where K_{15} , K_{16} , K_{18} , K_{19} are the rate constants of Reaction 15, 16, 18 and 19, respectively.
 5 σ_{N_2O} is the absorption cross-section of N_2O and ϕ_{N_2O} is the photolysis quantum yield. The
 6 values for them can be found in previous study (Kurten et al., 2012).

7 Ideally, the N_2O actinometry experiment should be conducted with the same flow rate as in the
 8 H_2O photolysis experiment such that the reaction time can be the same. However, at the flow
 9 rate suitable for CIMS calibration (10 slpm), the concentration of NO_x produced from N_2O
 10 photolysis is near the detection limit of the NO_x detector. Hence, the N_2O actinometry
 11 experiment was carried out at a lower flow rate (3 and 6 slpm) to increase the reaction time for
 12 photolysis and then the NO_x production. The It values for lower flow rate (It_{LOW}) and higher
 13 flow rate (It_{HIGH}) have the following relationship:

$$14 \quad It_{HIGH} = \frac{FR_{LOW} \times It_{LOW}}{FR_{HIGH}} \quad (E5)$$

15 where FR_{LOW} and FR_{HIGH} represent different flow rate. Based on this equation, It_{HIGH} can be
 16 obtained by scaling It_{LOW} with the ratio of FR_{LOW} and FR_{HIGH} . The E5 is validated in the next
 17 section.

18 **4.3.2 It determination**

19 Figure 3 shows the results of N_2O actinometry experiment. Figure 3a shows the NO_x produced
 20 as the function of N_2O mixing ratios from 10% to 15% at different flow rates ($FR_{N_2O} = 3, 6,$
 21 and 10 slpm). Generally, an increase in the N_2O mixing ratio or a decrease in reaction time
 22 (lower flow rate) led to more production of NO_x . In figure 3b, the product It corresponding to
 23 different flow rate was calculated according to E4 based on the result in Figure 3a. The product
 24 It linearly increased with the inverse of the flow rate, which validates the linear dependency
 25 between product It and inverse of the flow rate shown by E5. This linear dependency is
 26 consistent with the result in Kurten et al. (2012). In addition, the product It was independent of
 27 the N_2O mixing ratios in range of 10% to 15% (Figure 3c). Based on the E5, the flow rate
 28 scaled It (It_{HIGH}) is calculated from It_{LOW} in Figure 3b multiplying the ratio of FR_{LOW} (3, 6,
 29 and 10 slpm, respectively) to FR_{HIGH} (10 slpm). The It varied from 1.37 to 1.53×10^{11} at

1 different flow rates and N₂O mixing ratios. The mean value of 1.46×10^{11} photon cm⁻¹ was
2 adopted for $I_{t_{HIGH}}$.

3 **4.3.3 Calibration result**

4 Figure 4 shows an example of a typical procedure for determining the calibration factor. The
5 instrument signals were continuously measured by adjusting H₂O concentrations without
6 changing other parameters. The different OH concentrations were calculated according to E3.
7 For each step, the signal intensities (in Hz) of HSO₄⁻ and NO₃⁻ were collected for 6 minutes with
8 3 minutes each for background mode and signal mode. The calibration factors were determined
9 from the calculated OH concentrations and signal intensities based on E2. The red dots in
10 Figure 4 represent the average calibration factors for every 6 minutes. The result shows that
11 the calibration factors different steps were very close, ranging from 1.60 to 1.69×10^{-10} , and
12 were independent of water vapor concentrations. The averaged calibration factor for our CIMS
13 is 1.64×10^{-10} molecule/cm⁻³.

14 **5. CIMS optimizations**

15 As shown in Figure 1, the CIMS system is complicated, and its performance is affected by
16 different parameters and components. In this section, we present the results of tests for different
17 types of ion sources and scavenger gases (propane and C₃F₆), comparison of primary ions
18 detection, and optimization of the instrument sensitivity and noise.

19 **5.1. Ion source**

20 Radioactive ion source (²¹⁰Po or ²⁴¹Am) and corona discharge source (corona ionizer) have
21 been used as the ion source in previous studies (Berresheim et al., 2000; Sjostedt et al., 2007;
22 Kukui et al., 2008). In this study, ²¹⁰Po and corona sources were compared.

23 ²¹⁰Po emitted alpha particles that interact with the carrier gas to quickly form thermalized
24 electrons and positive ions (Fehsenfeld et al., 1975). The formed electrons react with O₂ and
25 then HNO₃ to produce NO₃⁻ · (HNO₃)_m · (H₂O)_n reactant ions. ²¹⁰Po was used due to its low
26 OH interference and ease of installation. Corona ionizer generates NO₃⁻ by discharge formed
27 between a tungsten needle and a 1 mm diameter plate 3 mm from the needle tip (Kukui et al.,
28 2008). The corona source has the advantage of producing much higher concentrations of NO₃⁻ ·
29 (HNO₃)_m · (H₂O)_n primary ions compared with radioactive ²¹⁰Po or ²⁴¹Am foils, which leads
30 to higher concentrations of HSO₄⁻ and higher signal intensities (and higher sensitivities).
31 However, the corona discharge source is known to produce a significant amount of neutral

1 species including OH radicals (artificial OH), which means the noise is relatively high (Kukui
2 et al., 2008). We compared a ^{210}Po ions source and a corona source (Figure S1). The result
3 showed that the detection limit of the CIMS with the ^{210}Po ion source was lower than that with
4 the corona source due to larger noise in the corona source. We previously applied the corona
5 source in the same CIMS to measure peroxy radicals (RO_2 and HO_2), and the noise level was
6 acceptable compared to the ambient concentration of peroxy radicals. For OH measurement,
7 although a scavenger gas was added in the sheath flow to remove most artificial OH radicals,
8 the remaining interferences were still high compared to ambient OH concentrations.

9 In this study, ^{210}Po foils were chosen as the ion source in our CIMS system. It should be noted,
10 however, that a radioactive source like ^{210}Po often subjects to strict health safety regulations,
11 and the users need apply a permit to use and transfer the radioactive source. In addition, ^{210}Po
12 undergoes alpha decay to stable ^{206}Pb with a half-life of about 140 days. Therefore, in order to
13 keep stable signal intensities for primary ions, the ^{210}Po foils need to be replaced regularly.

14 **5.2 Scavenger gases**

15 As discussed in Section 3, scavenger gas is very important for OH measurement by CIMS.
16 Propane, C_3F_6 , and NO_2 have been used by different groups (Berresheim et al., 2000; Sjostedt
17 et al., 2007; Kukui et al., 2008). However, there have been no reports on comparisons of these
18 three scavenger gases. In this study, The first two were compared. (We could not purchase high
19 purity NO_2 due to health safety restriction in Hong Kong). The scavenger gas was added in two
20 positions for different purposes. In the sheath flow, the scavenger gas reduced the interference
21 of artificial OH from the ion source; in the sample flow, it terminated the OH conversion (in
22 the rear injector) and eliminated the ambient OH to determine background (in the front injector).

23 Figure 6 shows that 99.95 vol.% pure propane (Harvest Wise Gases (H.K.) Limited) added in
24 sheath flow could effectively (~80%) remove artificial OH radicals from the ion source with
25 the remaining contributing a low and stable signal at 97 m/z. For the OH removal efficiency of
26 in the sample air, propane could remove OH at 97.7% of OH even at the concentrations of two
27 orders of magnitude higher than ambient OH level (for more details, see Section 5.4.3). The
28 signal intensity of the primary ions was not affected by the added propane and kept stable
29 (Figure S2).

30 For C_3F_6 , although its OH removal efficiency was also high, it suppressed the signal intensities
31 detected by the mass detector. This suppression recovered after time when the detector was
32 new (figure not shown). However, when the detector was aged, such suppression triggered a

1 continuous decrease of the reagent signal as shown in Figure S2a. In this case, the change of
2 reagent ions detection signal can avoid such decrease (Figure S2b).

3 Based on the above test results and considering that propane is inexpensive and easy to
4 purchase, propane was selected as the scavenger gas for our CIMS.

5 **5.3 Primary ions detection**

6 Determination of the OH concentrations needs to use the signal intensities of NO_3^- ions
7 according to E2. Some previous researchers traced the NO_3^- ions on the signal intensities at 62
8 m/z (Kukui et al., 2012; Sjostedt et al., 2007; Tanner et al., 1997). We found that the
9 concentrations of NO_3^- in the inlet system were extremely high. Even though a small portion of
10 the NO_3^- ions were finally detected by the mass detector, the signals were still very strong. After
11 operating the CIMS with detecting the signal of NO_3^- ions at 62 m/z about half a year, all signals
12 from the channeltron detector dropped significantly which may be due to the accelerated aging
13 of the detector by the high concentrations of NO_3^- ions. Therefore, the isotopic signal ($\text{N}^{18}\text{O}_3^-$)
14 at 64 m/z was chosen to detect NO_3^- primary ions for extended operation. The signal intensity
15 at 64 m/z is lower than at 62 m/z by about a factor of 167.

16 **5.4 Instrument sensitivity and noise**

17 **5.4.1 Sensitivity optimization**

18 The sensitivity (S) of the CIMS instrument to the OH radicals depends on the reaction
19 efficiency of OH and SO_2 in chemical conversion region (f(CE)), the conversion efficiency of
20 H_2SO_4 to HSO_4^- in chemical ionization region (f(IE)), and the transmitted efficiency of HSO_4^-
21 from sample inlet to mass spectrometer system (f(TE)):

$$22 \quad S \sim f(\text{CE}) \cdot f(\text{IE}) \cdot f(\text{TE})$$

23

24 f(CE) is dependent on the reaction time and the SO_2 concentration of the conversion reactions
25 (R1-3). f(IE) is affected by the flow dynamics, which determines the mixing of flows, and the
26 electric field inside the ionization region, which forces the $\text{NO}_3^- \cdot (\text{HNO}_3)_m \cdot (\text{HO}_2)_n$ primary
27 ions to the center of the region for H_2SO_4 ionization. The f(CE) is related to the N_2 buffer and
28 the induces electric field in the pinhole area. In this work, the f(CE) is first optimized for the
29 maximum conversion of the ambient OH to H_2SO_4 by adjusting the SO_2 flow and the sample
30 flow rate. Then, to achieve best f(IE) for H_2SO_4 ionization, the flow dynamic and electric field

1 are optimized by adjusting the sample/sheath flow ratio and the voltages applied to sample and
2 sheath flow. Finally, the N₂ buffer flow rate and the voltages of the pinhole are adjusted to
3 control the f(TE) to determine the amounts of ions entering the detector. During the
4 optimization, the calibration tube is applied to produce OH radical and control its concentration.

5 **5.4.2 Conversion efficiency**

6 Figure 5a shows the normalized signal intensity (NSI) at 97 m/z for HSO₄⁻ as a function of the
7 flow rate of SO₂ (0.9 vol.%). The NSI first increased with increased SO₂, and reached a stable
8 level at a flow rate > ~2.5 sccm, which did not vary with the relative humidity. This result
9 indicates that the SO₂ concentration at the flow rate of 2.5 sccm was adequate to convert
10 sampled OH to H₂SO₄. Since the concentration of OH radical produced by the calibration unit
11 during optimization was 1 to 2 magnitude higher than in that in ambient condition, the 2.5 sccm
12 flow of SO₂ is adequate for ambient measurement. We set the SO₂ flow rate at 5 sccm with a
13 factor of 2 margin, following the previous study (Sjostedt et al., 2007). With this flow rate, the
14 concentration of SO₂ in sample flow is 12 ppm.

15 The effects of the sample flow rate on NSI are shown in Figure 5b. During adjusting the sample
16 flow rate, if the sheath flow rate remains the same, the conversion time and the flow dynamics
17 will be affected. Thus, in order to show the effect of conversion time to NSI only, the sheath
18 flow was adjusted along with the sample flow to maintain the sample/sheath flow ratios and
19 control the f(IE) in Figure 5b. Briefly, the NSI increased with the decrease of sample flow rate,
20 which can be explained by a longer OH conversion time (R1-3) and a higher f(CE) at a lower
21 flow rate. However, the increased reaction time will also increase the OH interference produced
22 from HO₂ recycling in the presence of NO in sample air. Previous studies usually kept the
23 reaction time less than 60 ms to mitigate such interference (e.g. Tanner et al., 1997). After
24 considering the reaction time and interference, the sample flow rate was set at 3.7 slpm, which
25 gives a reaction time of ~47 ms. After the above selection of the SO₂ concentration and sample
26 flow rate, the optimal f(CE) is determined.

27 **5.4.3 Ionization efficiency**

28 Figure 5c shows the NSI as a function of the ratio of sample flow to sheath flow in the
29 ionization region. The NSI firstly increased and then decreased with the increased ratio, with a
30 peak value at a sample/sheath flow ratio of 0.3. This optimized ratio was independent of the
31 total flow rates from 12 to 21 slpm. This ratio produced a turbulent flow in the chemical

1 ionization region. Such flow dynamics facilitates a fast mixing of the reactants, and enhances
2 the $f(\text{IE})$ of H_2SO_4 as well as the NSI at 97 m/z (Tanner and Eisele, 1995; Tanner et al., 1997).
3 Figure 5d-e shows the effects of voltages applied to the sample and sheath flow on NSI. The
4 NSI first increased and then decreased as the increase of difference in voltage between the
5 sample and sheath flow (figure 5d). At the voltage difference of 48 V, the peak NSI was
6 achieved, and this voltage difference is selected. Figure 5e shows the NSI increased with the
7 negative sheath voltage and then kept stable with sheath voltage $< -70\text{V}$. This shows that when
8 it is negative charged, it is the voltage difference but not the exact voltage that affects the NSI.
9 In our studies, we set the inlet and sheath voltages at -32 and -80 V, respectively. The cross
10 interactions of sample/sheath flow and voltages on NSI were also evaluated (see Figure S3).
11 The result shows that the highest NSI was achieved when the sample/sheath flow ratio was
12 close to 0.3, independent of the voltages. The optimized $f(\text{IE})$ of the CIMS is achieved by the
13 above selections of the flow ratio and electric field.

14 **5.4.4 Transmission efficiency**

15 The N_2 buffer flow rate controls the proportion of sample air in dry N_2 (refer to figure 1),
16 thereby affecting amount of ion clusters in the sample air entering the mass detector. Figure 5f
17 shows that the NSI increased with the decreased the buffer flow rate, as expected. However, a
18 lower flow rate of N_2 buffer gas also allows more undesired neutral molecules and particles in
19 sample air to enter the mass spectrometer (Berresheim et al., 2000). With these considerations,
20 the flow rate of N_2 buffer gas was set as 440 sccm. To force the ions to the center of the pinhole,
21 the voltage applied to before and on the pinhole was set at -70V and -40V, respectively.

22 **5.4.5 Noise minimization**

23 After optimization of CIMS's sensitivity, noise minimization is needed to reduce the signal
24 that is not related to the ambient OH concentration. As discussed above, the noises for OH
25 measurements include H_2SO_4 in ambient air and artificial OH produced by the ion source.
26 These noises can be mitigated by adding a scavenger gas in the sheath flow to eliminate
27 artificial OH and in sample flow to quantify ambient H_2SO_4 (Figure 1). Below we determine
28 the optimal flow rates for the scavenge gas.

29 Figure 6 shows the HSO_4^- signal intensity as a function of propane flow rates in sheath flow,
30 with N_2 gas as the sample air. When propane was not added, the artificial OH concentration
31 from the ^{210}Po ion source was $\sim 3.5 \times 10^6$ molecules cm^{-3} , which is comparable to the typical OH

1 concentrations in ambient environments. When propane was added into the sheath gas, the
2 artificial signals were reduced with the increasing propane flow and kept stable at $\sim 1 \times 10^6$
3 molecules cm^{-3} when the flow rate was higher than 1 sccm. We thus set a flow rate of 2 sccm
4 for propane in the sheath flow.

5 Figure 7 shows the removal efficiency (RE) of OH by propane added in the sample flow as a
6 function of the propane flow rates. The OH radicals were produced by the calibration unit
7 described in Section 4.2. The RE increased with the increased propane flow rate initially and
8 levelled off at the flow rate > 1 sccm. We adopt the flow rate of propane of 2 sccm (~ 535 ppm),
9 which led to $\sim 98\%$ removal efficiency for OH. As OH concentrations in this test are much
10 higher than those in typical ambient air, the RE of the propane for ambient OH should be even
11 large at the selected flow rate.

12 **6. Detection limit and uncertainty**

13 The detection limit can be calculated as follows,

$$14 \quad DL = \frac{1}{C} \times \frac{n * \sigma}{\{\text{NO}_3^-\}} \quad (\text{E6})$$

15 Where DL is the detection limit in 10^6 molecule/ cm^3 , C is the calibration factor, and n is the
16 ratio of signal to noise S/N. σ represents the standard deviation of the signal intensity of HSO_4^-
17 at 97 m/z, and $\{\text{NO}_3^-\}$ represents the signal intensity of NO_3^- at 64 m/z at the integration time t .

18 Figure 8 shows the concentrations of OH radicals and the corresponding detection limit (S/N=2,
19 average time=6 minutes) in the laboratory. The detection limit was quite stable over the whole
20 day and ranged from 0.08 to 0.20×10^6 molecule cm^{-3} , with an average value of approximately
21 0.15×10^6 molecule cm^{-3} .

22 The uncertainty for the calibration factor (C) of OH measurements is dependent on the
23 uncertainties of all the parameters involved in the calculation of the concentrations of OH
24 radicals and the precision of the measurements of signal at 64 m/z and 97 m/z. The uncertainty
25 was $\sim 36\%$ for It (see Figure 3), $\sigma_{\text{H}_2\text{O}} \sim 5\%$ for $\sigma_{\text{H}_2\text{O}}$, $< 1\%$ for $\phi_{\text{H}_2\text{O}}$ (Cantrell et al. 1997), and
26 $\sim 10\%$ for the water concentration (Kukui et al., 2008). The precision of the measurements
27 signal at 64 m/z and 97 m/z of the CIMS instrument (2σ) was 11% (for 6 min integration time).
28 The overall uncertainty for the calibration factor was about 38%.

29 **7. Field deployment of CIMS**

1 In order to examine the performance of our CIMS in the ambient environment, we deployed
2 the optimized instrument to an urban site of Hong Kong in April 2019 (Figure S4). The site
3 was located on the 11th floor of a teaching building on the campus of The Hong Kong
4 Polytechnic University (PolyU) and was surrounded by several busy roads. The sample inlet
5 was positioned horizontally facing the south. Measurements were made with a time resolution
6 of 10 seconds. A typical measurement sequence consisted of 3 minutes in the background mode
7 and 3 minutes in the signal mode. Figure 9a shows the diurnal profile of OH concentrations (3-
8 minute average) observed on April 25, 2019, and the solar radiation measured using UTA-
9 LI200 at a time resolution of 1 minute. Figure 9b shows the measured signal intensities at 97
10 m/z at the signal mode and the background mode. The OH concentrations exhibited a clear
11 diurnal profile with the highest value of $\sim 6 \times 10^6$ molecules cm^{-3} at midday and the lowest level
12 of $\sim 0.25 \times 10^6$ molecules cm^{-3} at night. The OH concentrations were highly correlated to solar
13 radiation, which was similar to previous studies (e.g. Rohrer and Berresheim, 2006; Tan et al.,
14 2017). The 3-minute average OH concentrations were above the detection limits ($0.5\text{-}2 \times 10^6$
15 molecules cm^{-3}) most of the daytime, except during a cloudy period (08:00 to 10:00) (Figure
16 9a). This preliminary result demonstrated the capability of our CIMS for measuring ambient
17 OH on a clear day in an urban environment. However, Figure 9b reveals that the contribution
18 to instrument background from ambient H_2SO_4 was significant at the site, which raised the
19 detection limit and measurement uncertainty (to 51%). The ambient H_2SO_4 concentration (10
20 sec average), which was estimated by the normalized background signal divided by the OH
21 calibration factor, varied from 2.6×10^5 in before sunrise to 8×10^6 molecule/ cm^3 in mid-day
22 (figure not shown). Future work will make use of isotopically labelled $^{34}\text{SO}_2$ to eliminate
23 H_2SO_4 interference (Eisele and Tanner, 1991).

24 **8. Summary and conclusions**

25 To measure the atmospheric OH radicals, we have developed the first chemical ionization mass
26 spectrometry (CIMS) system in Asia. It is an indirect measurement technique that converts OH
27 radicals to HSO_4^- which is detected by the ion-assisted mass spectrometry method. In addition,
28 the calibration system has been developed. A series of comparisons of different ion sources,
29 scavenger gases, and primary ions detection have been conducted to optimize the performance
30 of the CIMS for OH measurement. The sensitivity is dependent on the efficiencies of
31 conversion reaction, ion conversion, and ion transmission which have been improved by
32 optimizing the flow rates of a myriad of gases and voltages in various components. An initial

1 field test has demonstrated the capacity of this instrument in measuring ambient OH in an urban
2 site on clear days. The main findings on the key parameters are summarized below.

3 (1) ^{210}Po has lower artificial OH interference compared to a corona ionizer, and it is
4 adopted as the ion source.

5 (2) C_3H_8 is a better OH scavenger than C_3F_6 because of the high elimination efficiency and
6 signal stability of C_3H_8 .

7 (3) A set of procedures has been developed to optimize the flow rates of sample gas, sheath
8 gas, and N_2 buffer gas, voltages on the sample inlet system and the concentration of
9 SO_2 conversion gas with the aim to increase instrument's sensitivity and reduce noise.

10 (4) The CIMS instrument achieved a detection limit of 0.15×10^6 molecules cm^{-3} and
11 uncertainty of 38% (S/N=2) under laboratory conditions. In the field, the detection
12 limit increased to about 0.15×10^6 molecules cm^{-3} on clear days, with the overall
13 accuracy of about 51%.

14 (5) Future work includes more field experiments in various environments and utilization
15 of isotopically labelled $^{34}\text{SO}_2$ to eliminate the H_2SO_4 interference.

16 We note that the optimal values of instrument parameters may differ in different CIMS systems
17 due to the different design and/or configurations, the test procedures and results from our study
18 provide a useful reference to other researchers who wish to apply CIMS technique to measure
19 atmospheric OH radicals.